TWO-PHASE FLOW

Robert R. Tacina
NASA Lewis Research Center
Cleveland, Ohio

An experimental program to characterize the spray from candidate nozzles for icing-cloud simulation is discussed. One candidate nozzle, which is currently used for icing research, has been characterized for flow and drop size. The median-volume diameter (MVD) from this air-assist nozzle is compared with correlations in the literature. The new experimental spray facility is discussed, and the drop-size instruments are discussed in detail. Since there is no absolute standard for drop-size measurements and there are other limitations, such as drop-size range and velocity range, several instruments are used and the results are compared. The drop-size instruments used are the Malvern 2600, the NASA Lewis Scanning Radiometer, the Phase/Doppler Spray Analyzer (P/DSA), a Forward-Scattering Spectrometer Probe (FSSP), an Optical Array Probe (OAP), and a limited amount of photography. The known capabilities and limitations of the drop-size instruments are compared.

A two-phase model was developed at Pennsylvania State University. The model uses the $k-\epsilon$ model of turbulence in the continous phase. Three methods for treating the discrete phase are used: (1) a locally homogenous flow (LHF) model, (2) a deterministic separated flow (DSF) model, and (3) a stochastic separated flow (SSF) model. In the LHF model both phases have the same velocity and temperature at each point. The DSF model provides interphase transport but ignores the effects of turbulent fluctuations. In the SSF model the drops interact with turbulent eddies whose properties are determined by the $k-\epsilon$ turbulence model. The two-phase flow model has been extended to include the effects of evaporation and combustion. Model development has been accompanied by an experimental program to provide data for verification. Presently, the model has been further extended at NASA Lewis to include the effects of swirling flow, and a particle-laden swirling flow experiment is currently being performed to provide verification data.

INTRODUCTION

Sprays and two-phase flow are of interest in many fields - for example, gas turbine combustion, agricultural crop spraying, paint spraying, fire protection, and drying. This paper describes the use of sprays to simulate icing clouds for the Altitude Wind Tunnel Icing Research Program. Icing-cloud simulation and gas turbine combustion research have common interests in the method of injection, the characterization of drop size and of droplet velocities, and the development of analytical models for droplet trajectories and droplet vaporization. This paper discusses injector or spray-nozzle drop-size characterization, an experimental test facility for injector characterization, drop-size measurement techniques, and analytical models for trajectory calculations.

INJECTOR CHARACTERIZATION

The injector, or spray nozzle, used currently for icing-cloud simulation at the NASA Lewis Research Center is an air-assist injector (fig. 1). It is

very similar to the injector used by Nukiyama and Tanasawa (ref. 1). The water flows through a center tube (0.635-mm diam) and has a concentric annular passage (9.35-mm diam) for air-assist flow. The water and the air exit through a 3.175-mm orifice. The advantage of an air-assist injector for icing research and other applications is that, within limits, there is nearly independent control of water flowrate and drop size. The water flow is controlled by the difference between the air pressure and water pressure, and the drop size is controlled by the air pressure only.

Drop-size measurements using this injector were made for us at Arnold Engineering Development Center by J.L. Hunt. The drop-size data shown in figure 2 are plotted as median-volume diameter in micrometers. The median-volume diameter MVD is defined as the drop size where 50 percent of the total droplet volume is contained in droplets less than that diameter, and 50 percent is contained in droplets greater than that diameter. The MVD is plotted as a function of the difference of water and air-assist pressure with the air-assist pressure as a parameter.

This method of correlating the data is very useful for setting the operating conditions in the wind tunnel. However, the drop-size data could be presented in a more fundamental manner as a function of the water to air mass ratio. Other factors that appear in correlations in the literature, such as viscosity, surface tension, and relative velocity between the air and water, are constant or nearly constant for these data. The relative velocity is nearly constant, even though the flowrates are changing. The reason for this is, first, that the air is being injected at high pressure into a low-pressure ambient environment and thus has sonic, or nearly sonic, velocity. Second, the water pressure is relatively low so that the water has a relatively small velocity compared to the sonic velocity of the air. Thus, the difference in the velocities or the relative velocity is constant.

These data were compared to values from various correlations. These comparisons are shown in figure 3 for one air-assist pressure. The injectors used in the references were similar to the NASA Lewis Research Center injector. However, the drop-size measurement techniques were different. The Nukiyama-Tanasawa (ref. 1) drop-size correlation was made from measurements of water droplets on photographs. The Lorenzetto-Lefebvre correlation (ref. 2) was made from light-scattering measurements of water droplets. Wigg (ref. 3) used measurements from molten wax sprays with swirl. As you can see in the figure, the results of the correlations have a wide range of values, some higher and some lower than the data taken at Arnold. Preliminary data taken at NASA Lewis seem to be closest to the data of Nukiyama-Tanasawa. Preliminary data taken with the NASA Lewis injector at Carnegie-Mellon University are lower than the Arnold data. There needs to be much more work on drop-size measurements and correlations before drop sizes can be accurately predicted.

TEST FACILITY

The objectives of our experimental program are to characterize a variety of candidate injectors for drop size and dispersion, to compare different drop-size measurement techniques, and to take data that can be used for trajectory models. Trajectory model data consist of initial condition data taken upstream close to the injector and verification data taken far downstream.

The test stand is shown in figure 4. Duct air enters through a 40-cm-diameter pipe. The maximum air velocity through the pipe is 88 m/sec. We will be able to control the relative humidity from 0 to 100 percent by adding steam far upstream. Controlling the relative humidity could be necessary if evaporation is important.

The duct air temperature will be controlled by injecting liquid nitrogen upstream. The primary use of the temperature control will be to provide a constant inlet temperature of 292 K. For some icing tests the inlet temperature is held at 273 K and even lower temperatures for shorter times.

The injector is inserted in a section with a window so that the nozzle operation can be monitored with a television camera. Water is the only liquid capable of being tested in this facility. The water is demineralized and heated to 380 K. For icing applications, the water and the air-assist injector are heated so that ice crystals do not form during the expansion process. The water and air-assist flow temperature can be controlled between the ambient temperature and 373 K.

The injector is shown in a section 2.5 m upstream of the instrument section. The injection section can be moved to any location closer to the instrument section. Upstream of the injector there is a traversing pitot tube to measure the inlet velocity.

Downstream, at the instrument section, drop-size measurements can be made. The instrument section has a square cross section with windows in the sides that are at 7° angles to each other to prevent reflections. Other drop-size instruments that are used are described in the next section. The instruments sit on a three-axis traversing table so that radial and spatial variations can be measured. A liquid-water measurement probe traverses vertically to measure the variation in liquid-water concentration.

Another set of droplet-sizing instruments is mounted in the duct downstream of the instrument section. The principle of operation of these instruments is discussed in the next section. These instruments are intrusive and mounted in a fixed position. They are the same instruments that are mounted on airplanes to measure drop sizes in clouds. Tests with these instruments will provide a good comparison of the data from the nozzles with that in the clouds. This is an atmospheric pressure rig, so the air and water are vented to the atmosphere.

DROP-SIZE INSTRUMENTS

The most important factor in making drop-size measurements is the drop-size measuring instrument. As you have seen from the figure comparing the drop-size data correlations, there must be large differences in the data on which they are based. One of the major problems is that there is no standard to which to compare the drop-size measurements, especially in a spray. Since there are other limitations beside the lack of a standard such as drop-size range and velocity range, in our program we use five different drop-size instruments and compare the results. The instruments are a Malvern 2600, a NASA Lewis Scattered-Light Scanner, a Phase/Doppler Spray Analyzer, a Forward-Scattering Spectrometer Probe, and an Optical Array Probe. And a limited

amount of photography is used for qualitative analysis. A qualitative analysis and a discussion of each of these instruments follows.

The Malvern 2600 is a commonly used drop-size instrument (fig. 5). Lewis' HSD version of this instrument, which provides a faster snapshot of the data, is described in reference 4. (The inserts in figure 5 describe the principle of operation.) This instrument measures the angle that the light is diffracted by the drops. The bigger drops diffract the light at a small angle and the smaller drops diffract the light at a larger angle. The detector is a series of concentric rings that determine the angle of the scattered light. The drop size is calculated from the scattered light angle. The insert also shows that, no matter where the droplet is in the line of sight, the light that is scattered at the same angle always falls on the same detector ring.

Although there is no standard for determining drop sizes, we use a Hirleman reticle for calibration purposes. The Hirleman reticle (fig. 6) consists of a glass substrate on which chrome disks are photographically deposited. The chrome disks are sized to represent a Rosin-Rammler distribution with an x-bar of 50 and an n value of 3. One problem we have found using the reticle with the Malvern 2600 is that there is a correction for anomalous diffraction. The Malvern calculations are based primarily on Fraunfaufer diffraction theory. However, for small drop sizes (below a diameter of 5 μm) three-dimensional effects are considered; these effects are lumped under the term anomalous diffraction. Thus, the problem is that the reticle has two-dimensional disks and not three-dimensional spheres. We are currently studying the feasibility of modifying the Malvern software to ignore the anomalous diffraction calculation when using the reticle. If this does not prove to be practical, we will still use the reticle for relative comparisons.

We also plan to add an additional lens system to the Malvern to be able to measure an MVD of 5 μm across the 30-cm instrument section. Verification of the correctness of the additional lens system will be done by taking measurements of the reticle with and without the additional lens system.

The second instrument, the Scattered-Light Scanner, is also based on the diffraction principle. This is a revised version of the NASA Lewis Scanning Radiometer (described in ref. 5), which was developed by Don Buchele and used in many research projects by Robert Ingebo. Figures 7 to 9 explain the operation of the instrument.

Figure 7 shows the reflection, refraction, and diffraction of a laser light beam passing through a drop. Since calculations are based on the diffraction of light through the drop, the wide-angle diffraction is ignored. There is narrow-angle diffracted light from the envelope (or aperture) of the laser beam that must also be ignored.

Figure 8(a) is a plot of light intensity as a function of the light-scatter angle. Figure 8(b) shows the product of the light intensity and the light-scatter angle as a function of the light-scatter angle. It shows that the measurement interval extends from where the intensity of the near envelope diffraction is negligible to a value of the light intensity which is still high enough to be meaningful. A scanner is used to measure the intensity of the scattered light as a function of the light scatter angle. The scanner is a

disk with a radial slot that is rotated with its centerline eccentric to the laser beam centerline.

To calculate the mean drop size, Don Buchele has calculated the light intensity as a function of a beam spread parameter (fig. 9). From the previous figure we can find the maximum light intensity and the light intensity at a specified angle. Using these values and the beam spread parameter and knowing the wave length and the specified angle, we can determine the mean drop size. Calculations were made with five different distribution correlations, and they are shown plotted for three dispersion levels. The distribution correlations used were the Nukiyama-Tanasawa, the upper-limit distribution functions, the Rosin-Rammler, the Weibel, and the Rinks distribution function. The beam-spread parameter is nearly the same for all the distributions and dispersions at a relative intensity of 0.75. If this relative intensity is used, then the mean drop-size calculation is independent of distribution and dispersion. The dispersion can be calculated from the slope of the curve.

A schematic of the Scattered Light Scanner (fig. 10) shows the various parts and dimensions of the instrument. The primary feature is the eccentric light scanner.

The third drop-size instrument to be discussed was developed under a NASA combustion fundamentals contract to William Bachello at Aerometrics Corporation. The method is the phase/Doppler detection technique and the instrument is called the Phase/Doppler Spray Analyzer (ref. 6). This is a scheme where a set of laser beams is crossed to form a fringe pattern (fig. 11). As a droplet passes through the fringes the light is scattered and measured 30° off axis with a photodetector. From this measurement, simultaneous values of drop diameter and velocity can be calculated. The measurement and calculations are for single droplets; averages and medians are calculated from the single droplet data.

Figure 12 shows in more detail the principle of the phase/Doppler system. The scattered light is collected by three detectors with slightly different spatial locations. Because of the spatial difference, the light path to the three detectors is different, and thus there is a phase difference in the signals. From this phase difference the drop size can be calculated. Again, the phase difference occurs because of the path difference inside the drop, so that the phase angle is a function of the diameter.

Figure 12(b) is a plot of phase difference as a function of diameter. From the phase difference between detectors 1 and 2, an approximate drop-size estimate can be made. From this approximate drop size and the phase difference between detectors 1 and 3, a more accurate determination of diameter can be made.

The calculations are based on reflection and refraction theory. Diffraction can be ignored because the measurements are taken 30° off axis, where diffraction is negligible.

The Forward-Scattering Spectrometer Probe (FSSP) is one of the two intrusive instruments that we use that is located downstream of the instrument section. This instrument is the same type that is mounted on airplanes to measure raindrop diameters (see ref. 7). It provides a comparison of the other drop-size instrument measurements with the measurements made in clouds.

The FSSP is a single particle counter. A schematic of its operation is shown in figure 13. A laser beam is optically directed across two arms of the probe, in a direction perpendicular to that of the particle-laden flow. Scattered light from a particle is optically directed and focused onto a photodiode to measure the intensity of the scattered light. Any unscattered light is removed by the dump spot. The scattered light is also directed onto a second photodetector that is used to determine whether the droplet is in focus (in focus along the axial length of the laser beam). This second photodetector also has a dump spot. The light from a droplet that is in focus is removed by the dump spot. A droplet that is not in focus has a broader signal that is not removed by the dump spot, and the droplet measurement is rejected.

Drop size as a function of the measured intensity is shown in figure 14. In the figure the light intensity is shown in the near forward-scattering angles of 4° to 14°. The curve is shown for a Gaussian T-type (transverse electric) beam. This is a multivalued function; thus, for a given intensity, the drop size may not be uniquely determined. The actual instrument uses a high-mode laser beam which has a smooth curve and is single valued.

The last drop-size instrument to be discussed is the Optical Array Probe (OAP), which can also be flown on an airplane to measure raindrop sizes. This instrument is made by the same company as the FSSP, but it is made to cover a larger drop-size range. The operating principle is shown in figure 15. It is a single-particle imaging system. The drops pass through a laser beam, and then the light is transmitted through the instrument optics to an array of photodetectors. The drop size is determined by counting the detectors in the shadow of the drop. The last detector at each end is kept open as a check to determine if the whole drop is seen. To determine if the drop is in focus, we use an intensity gradient criteria. An infocus drop has a sharp gradient from lit to unlit photodetectors, while an out-of-focus drop has a gradual gradient from lit to unlit. Figure 16 is a simple schematic of the OAP.

Table I compares the FSSP, OAP, Malvern 2600, Scattered-Light Scanner, and Phase/Doppler Particle Analyzer (P/DSA) drop-size instruments. The size range refers to the droplet diameters that can be measured with any particular setup. The number of bins refers to the number of increments into which the size range is divided. The overall size range then refers to the smallest to the largest diameter that can be measured, but it may require a change in setup and multiple measurements to cover the range. The numbers in the ranges refer to individual droplets for all the instruments except for the Scattered Light Scanner, whose range is given in MVD.

The velocity limits are all acceptable for our work except for those of the P/DSA, which has a slight limitation for our purposes. Currently manufactured P/DSA instruments have a upper limit of 75 m/sec. The comments section lists features that we consider particularly beneficial. With the FSSP and OAP, we consider the ability to use the same instrument to obtain data from clouds and the test facility to be important. The Malvern and the Scattered-Light Scanner have the ability to measure MVD directly and thus are good for screening a number of injectors quickly. The P/DSA has the capability of making point measurements of size and velocity which makes the data particularly useful for modeling work.

68

ANALYTICAL TRAJECTORY MODELS

The second part of this report describes spray model development. The model work to be presented was done at Pennsylvania State University by Professor Faeth and his graduate students and associates (refs. 8 to 10). Figure 17 shows the important interactions of the drop with its environment. These interactions are: the droplet drag that results in a source term in the continuous flow equation, random deflections of the drops by turbulent eddies, and turbulence modulation of the continuous phase by the extraction of turbulent energy by the droplet drag. Actually, three models of increasing complexity were developed. They are a locally homogenous flow model, a deterministic separated-flow model, and a stochastic separated-flow model.

The locally homogenous flow model is the simplest model (fig. 18). It uses the k-ε model to calculate the continuous-phase flow characteristics. It then assumes that the particles have the same velocity as the continuous phase and treats the k-ε equations as a varying-density flow. This model is correct for small drops that follow the continuous phase flow. An advantage of the model is that the calculation is no more complex for a two-phase flow than for a single-phase flow. It is also useful when the initial conditions of the spray, such as drop size or spray angle, are not available since they are not needed in the calculation.

The second model is the deterministic separated flow (DSF) model (fig. 19). It also uses the k-ε model to calculate the gas or continuous-phase flowfield. The particle or droplet distribution is divided into a number of classes with a representative number of droplets in each class. Then, for each drop, the trajectory is calculated. The trajectory calculation is based on the mean continuous-phase flow properties. Dispersion due to turbulence is ignored. This is the most widely used approximation in current models of combusting sprays. Other assumptions are that the drops are spherical and that the spray is dilute with no collisions.

One feature of this model is the particle-in-cell approach. As a particle goes through a cell, the drag momentum is coupled with the continuous-phase momentum. The net change in momentum is calculated for each drop class as it passes through a computational cell as shown in figure 20. Then the gas or continuous-phase flow equation is calculated with the change in momentum as a source term.

The last, and most complex, model is the stochastic separated flow (SSF) model (fig. 21). In this model, the continuous-phase turbulence does interact with the drop or particle. Again the gas-phase calculation is made using the k-ε model. To make the Lagragian drop-trajectory calculation we assume the drop interacts with an eddy. The properties of the eddy have a distribution based on a probability density function with a standard deviation dependence on k. From the distribution, the properties of the eddy are found by using a Monte Carlo technique. The interaction is shown in figure 22. The drop interacts with the eddy either for the lifetime of the eddy or the time it takes the particle to traverse the eddy. The size of the eddy is based on the dissipation length. The number of calculations are much greater for this

method than for the deterministic separated flow (DSF) model. While for the DSF model approximately 600 drops are sufficient for an accurate calculation, for the stochastic separated flow model about 6000 drops are needed for an accurate calculation.

An experimental study was also done to complement the analytical modeling effort. From a large amount of data, four plots were chosen as representive. Figure 23 is a plot of the mean axial velocities of the drops as a function of the drop diameter at different axial locations. An air-assist injector with an exit-orifice diameter of 1.194 mm was used. The initial conditions were taken at an x/d of 50, where x is the axial distance and d is the injector-orifice diameter. This is a distance of about 55 mm. This was sufficient distance for the spray to be well formed for most conditions. However, there were some conditions where ligaments were observed.

The drop-size and velocity measurements were made using double-flash photography. Two other methods were used to measure drop size. One was slide impaction in which a slide coated with magnesium oxide was used. The second alternate method was to measure drop size with a Malvern. The Malvern measurement was used mainly to monitor the spray to determine whether the spray varied from day to day.

The data were compared with the calculations from the stochastic separated flow model and the deterministic separated flow model. The calculations agree well, with the data from the stochastic separated flow model agreeing the best. For all the data plots, the stochastic separated flow model agreed well with the data, while the deterministic separated flow model and the locally homogenous model agreed well for some conditions and not so well for other conditions.

Figure 24 shows the radial variation of mean liquid flux G. For this case, the SMD at an x/d of 50 was 30. Again the calculations with the stochastic separated flow model agree well with the data for all conditions, while the other two models do not agree well for all conditions. It is interesting to note that the locally homogenous model underpredicts the data. For all the previous work in which the locally homogenous model was calibrated with solid-particle-laden flow, the model overpredicted the development of the spray.

Figure 25 shows the variation of the Sauter mean diameter with the distance along the axis. Figure 25(a) is for a nonevaporating oil spray and figure 25(b) is for an evaporating Freon 11 spray. Case 1 had an initial SMD of 30 at an x/d of 50 and case 2 had an initial SMD of 87. For the nonevaporating case, the mean diameter increases after an x/d of 100 because of the greater dispersion of the small drops. The stochastic separated flow model does better at predicting the data because it considers the dispersion due to turbulence.

The variation of SMD along the axis for an evaporating spray is shown in figure 25(b). For an evaporating spray, there are competing effects: evaporation reduces the mean diameter, and greater dispersion of the small drops increases the mean diameter along the axis. The stochastic separated flow model and deterministic separated flow model do a good job of predicting the trends even if they do not exactly duplicate the data.

70

The model development is continuing at the NASA Lewis Research Center as part of a Ph.D. thesis (by Daniel Bulzan). The ability to calculate flow fields with swirl has been added to the model, and an experimental calibration and verification is underway. The experiment will have a weakly swirling flow field with a swirl number of less than 0.4. Glass beads with known sizes will be used to simplify the analysis. Particle number flux will be measured by a 30° off-axis Mie-scattering technique. Laser Doppler velocimetry (LDV) will be used to measure the particle and gas-phase velocities. The parameters to be studied are swirl number, particle loading ratio, and particle size. The initial conditions will be well characterized to provide input conditions to the computer model.

Figure 26 is a drawing of the experimental configuration. It has a two-component laser velocimeter system that will be used to measure the particle and the gas-phase velocities. Small aluminum oxide particles, approximately 0.5 μm diameter, will be added to make the gas-phase velocity measurement. The laser system will remain fixed and the injection system will be traversed to determine spatial variations. The injector has four tangential slots to create swirl.

CONCLUDING REMARKS

There has been much work in this field of two-phase flow in the past, and, with the new instruments that are more accurate, faster, and easier to use, there promises to be great advances in the experimental data base. Analytical models will complement the experimental work; there promises to be more accurate and faster analytical models to calculate the two-phase flow fields that exist in icing clouds, gas turbine combustors, and other applications.

REFERENCES

1. Nukiyama, Shiro; and Tanasawa, Yasushi (E. Hope, trans.): Experiments on the Atomization of Liquids in an Air Stream. Rept. No. 4, The Influences of the Characteristics of the Liquid on the Atomized Droplets. Defense Res. Board, Dept. Nat. Defense, Ottawa (Canada), Mar. 18, 1950. (Trans. from Trans. Soc. Mech. Eng. (Japan), vol. 5, no. 18, Feb. 1939, pp. 68-75.)

2. Lorenzetto, G.E.; and Lefebvre, A.H.: Measurements of Drop Size on a Plain-Jet Airblast Atomizer. AIAA Paper 76-679, July 1976.

3. Wigg, L.D.: Drop-size Prediction for Twin-fluid Atomizers. J. Inst. Fuel, vol. 37, no. 286, Nov. 1964, pp. 500-505.

4. Watson, D.J.: Laser Diffraction Measurements in Transient Spray Conditions. ICLASS-85, 3rd International Conference on Liquid Atomization and Spray Systems, Vol. 1, P. Eisenklam and A. Yule, eds., Institute of Energy, London, 1985, pp. VC/4/1 - VC/4/15.

5. Buchele, D.R.: Particle Sizing by Measurement of Forward-Scattered Light at Two Angles. NASA TP-2156, 1983.

6. Bachalo, W.D.; and Houser, M.J.: Phase/Doppler Spray Analyzer for Simultaneous Measurements of Drop Size and Velocity Distributions. Opt. Eng., vol. 23, no. 5, Sept.-Oct. 1984, pp. 583-590.

7. Knollenberg, R.G.: The Use of Low Power Lasers in Particle Size Spectrometry. Practical Applications of Low Power Lasers, SPIE vol. 92, D.D. Eden and J.S. Chivian, eds., SPIE, 1976, pp. 137-152.

8. Shuen, J-S., et al.: Structure of Particle-Laden Jets: Measurements and Predictions. AIAA J., vol. 23, no. 3, Mar. 1985, pp. 396-404.

9. Solomon, A.S.P., et al.: Measurements and Predictions of the Structure of Evaporating Sprays. J. Heat Trans., vol. 107, no. 3, Aug. 1985, pp. 679-686.

10. Shuen, J-S.; Solomon, A.S.P.; and Faeth, G.M.: Drop-Turbulence Interactions in a Diffusion Flame. AIAA J., vol. 24, no. 1, Jan. 1986, pp. 101-108.

TABLE I. - DROPLET-SIZE INSTRUMENT COMPARISON

	Forward-Scattering Spectrometer Probe, FSSP	Optical Array Probe, OAP	Malvern 2600	Scattered-Light Scanner	Phase/Doppler Particle Analyzer, P/DPA
Size range	1 to 16 2 to 32 2 to 47 5 to 95	20 to 300	1.3 to 128 1.9 to 188 5.7 to 564	6 to 120 MVD	$D_{max}/D_{min} = 35$
Number of bins	15	15	15	NA	68
Overall size range	1 to 95	20 to 300	1.3 to 564	6 to 250 MVD	1 to 1000
Velocity limits	5 to 100 m/sec	5 to 100 m/sec	None	None	3.2 x fringe spacing 41 m/sec
Measurement theory	Scattering amplitude	Particle shadow size	Fraunhofer diffraction	Fraunhofer diffraction	Geometric optics
Type of measurement	Single-particle counter	Single-particle counter	Ensemble average	Ensemble average	Single-particle counter
Probe volume	0.218-mm (diam) x 2.61 mm	4.8 mm (diam) x 6 cm	Line of sight x 9 mm diam	Line of sight x 50 mm or 18 mm	0.160 mm (diam) x 0.050 mm
Comments	Flight-instrument icing research		Measures volume distribution (best for MVD)		Size-velocity correlation

AIR-ASSIST FLOW

WATER
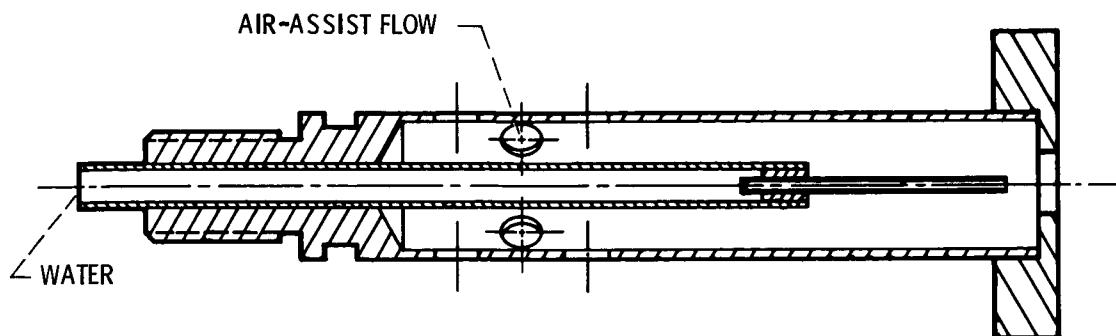
Figure 1. - IRT nozzle.

CD-85-17630

AIR-ASSIST
PRESSURE,
MPa
○ .17
□ .31
◇ .44
△ .58
▽ .78
◊ 1.05
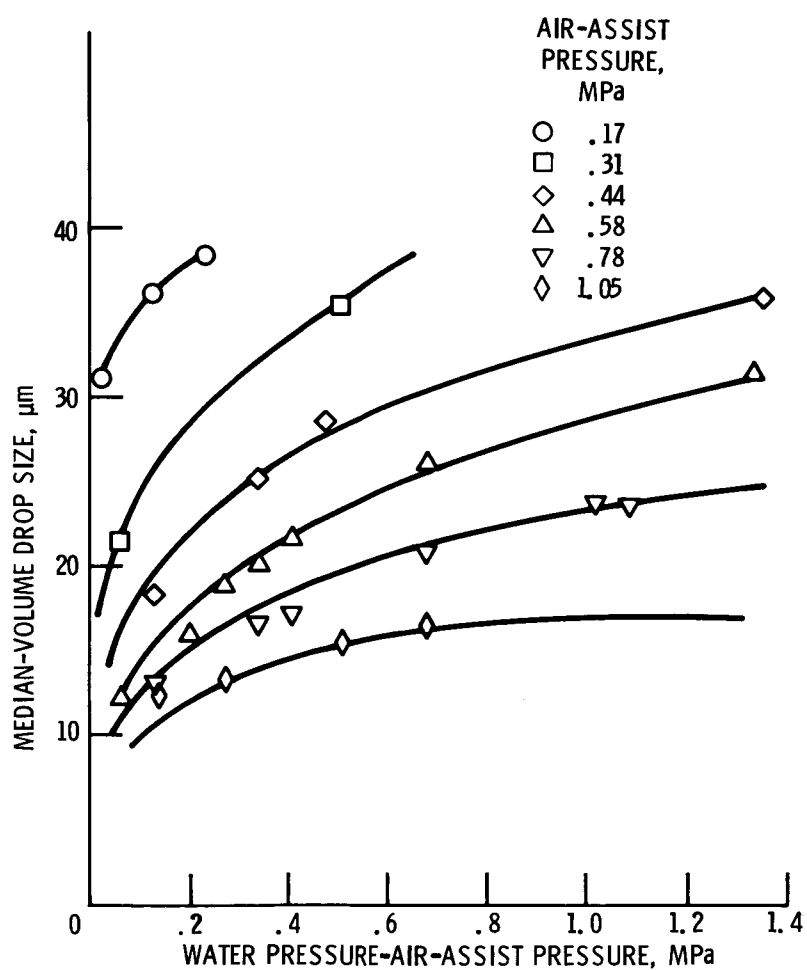
Figure 2. - Drop sizes from IRT nozzle.

CD-85-17394
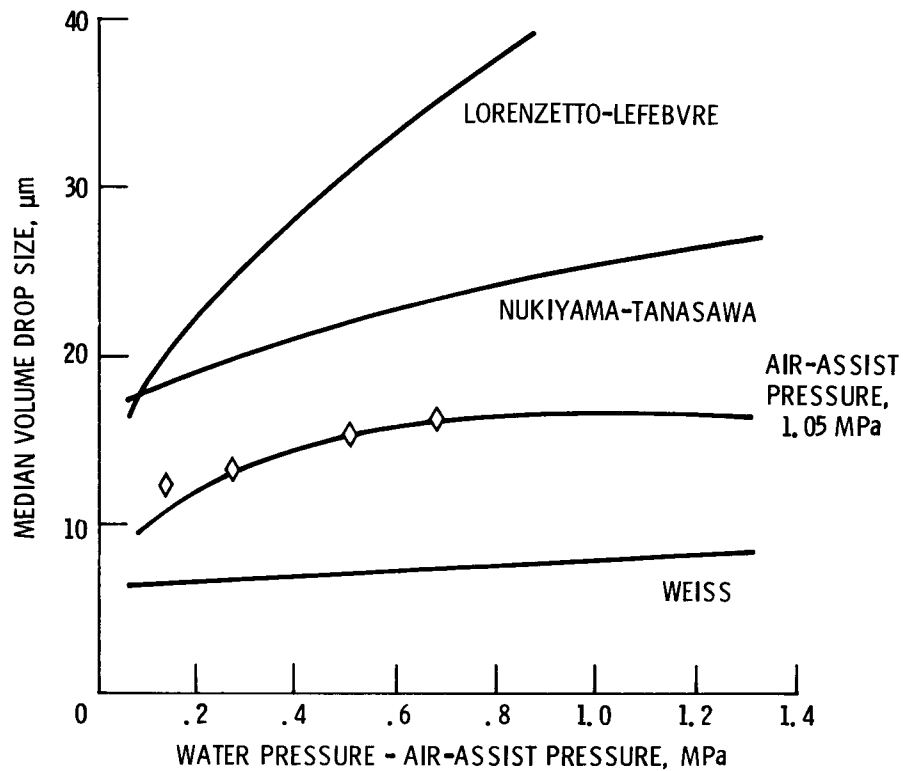
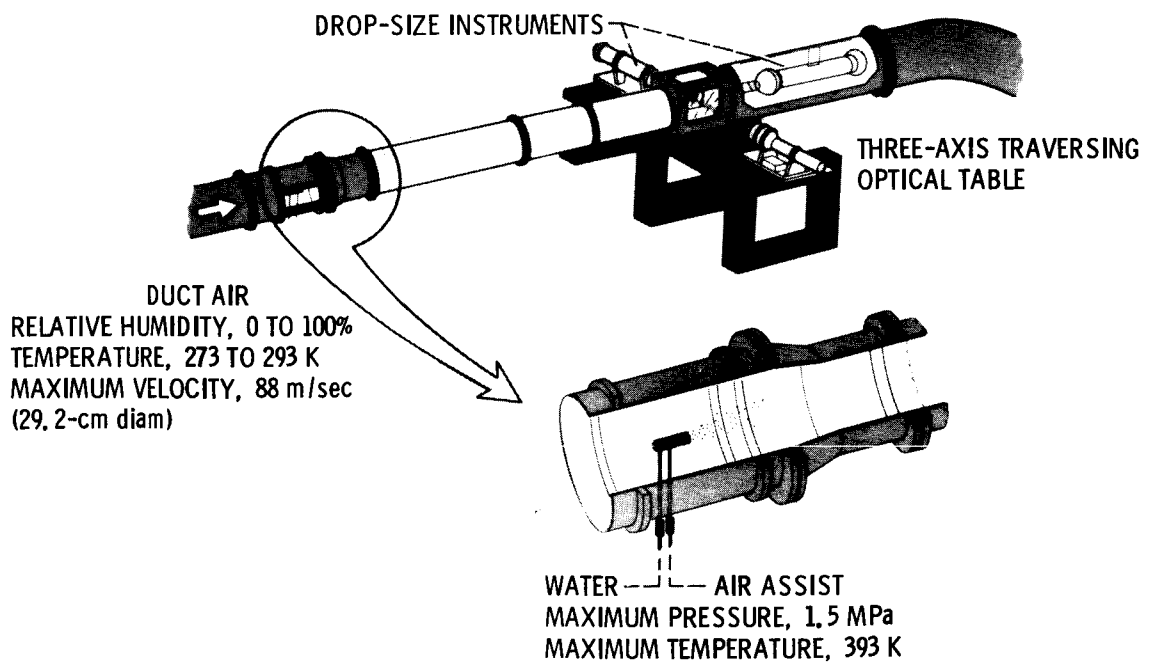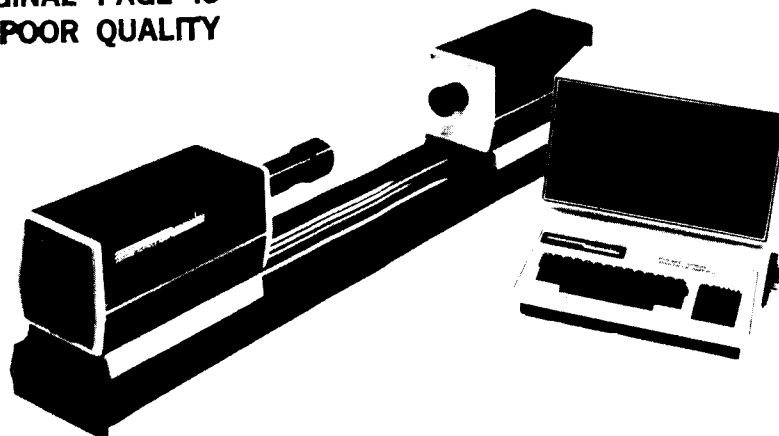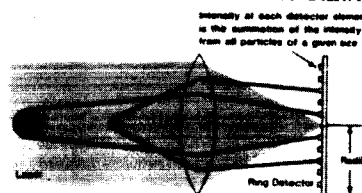Figure 3. - Comparison of IRT nozzle drop-size data with correlations.

CD-85-17628

DROP-SIZE INSTRUMENTS

THREE-AXIS TRAVERSING OPTICAL TABLE

DUCT AIR
RELATIVE HUMIDITY, 0 TO 100%
TEMPERATURE, 273 TO 293 K
MAXIMUM VELOCITY, 88 m/sec
(29.2-cm diam)

WATER ──┘└── AIR ASSIST
MAXIMUM PRESSURE, 1.5 MPa
MAXIMUM TEMPERATURE, 393 K

Figure 4. - Experimental spray facility.

74

PRINCIPLE OF DIFFRACTION SIZING   MEASURING MOVING PARTICLES

SMALL PARTICLES DIFFRACT LIGHT
THROUGH LARGE ANGLES AND
LARGE PARTICLES THROUGH SMALL
ANGLES
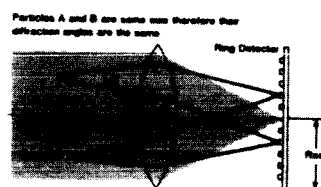
WHEN A FOURIER TRANSFORM
LENS IS USED, THE LIGHT DIF-
FRACTED BY PARTICLES OF A
GIVEN SIZE AT ANY POSITION
IN SPACE ALWAYS FALLS ON
THE SAME PART OF THE DE-
TECTOR

Figure 5. - Malvern spray analyzer.
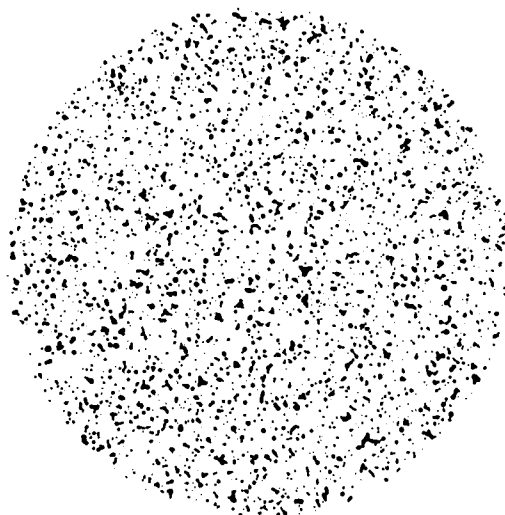
::::: SIZING
       ARRAY

Figure 6. - Photograph of sample area and quality control array of Hirleman
calibration reticle (RR-50-3.0-0.08-102-CF-#115). Magnification 10x.

CD-85-17399

WIDE-ANGLE REFRACTION THROUGH DROP, CAN BE NEGLECTED

MEDIUM-ANGLE DIFFRACTION AROUND DROP, $\theta = \lambda/\pi D$, MEASURED

SMALL-ANGLE DIFFRACTION NEAR ENVELOPE OF LASER BEAM, PREVENTS MEASUREMENT AT SMALL ANGLES
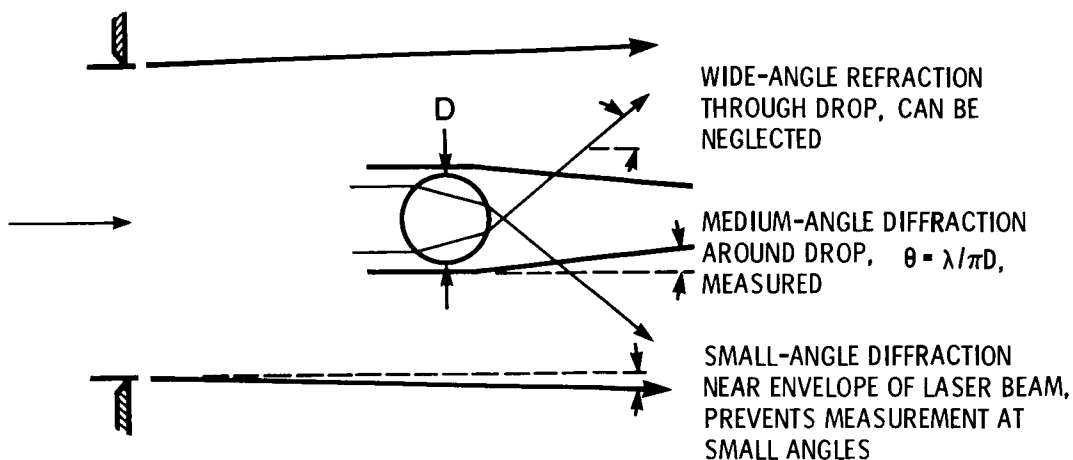
Figure 7. - Three principal components of scattered light at test section.

CD-85-17397

DIFFRACTION NEAR ENVELOPE OF LASER BEAM

DIFFRACTION AROUND DROP
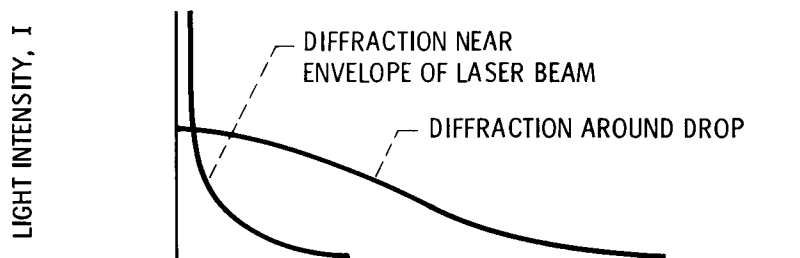
LIGHT INTENSITY, I

(a) Light intensity as function of light-scatter angle.

MEASURED INTERVAL

LIGHT INTENSITY x LIGHT SCATTER ANGLE, Iθ

1.0

.4

0

θMEASURED

LIGHT SCATTER ANGLE, θ
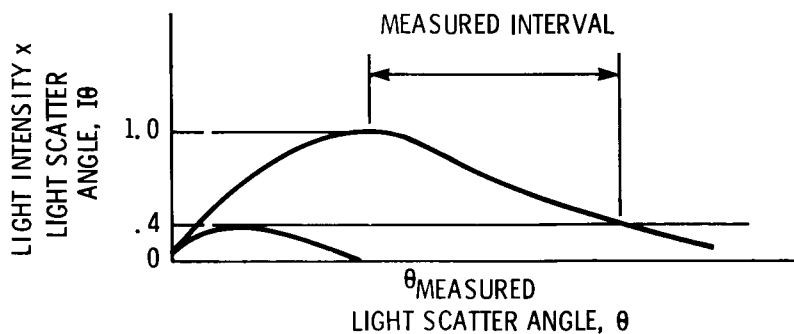
CD-85-17413

(b) Product of light intensity and light-scatter angle as function of light-scatter angle.

Figure 8. - Intensity of forward-scattered light.

76

DISPERSION $= 2(D_{.9} - D_{.1})/(D_{.9} + D_{.1})$

DISPERSION, 1.35

DISPERSION, 0.75

MONODISPERSE

RELATIVE INTENSITY, $I\theta/(I\theta)_{max}$

BEAM-SPREAD PARAMETER, $P = \frac{\pi}{\lambda} D_{v.5}\theta$
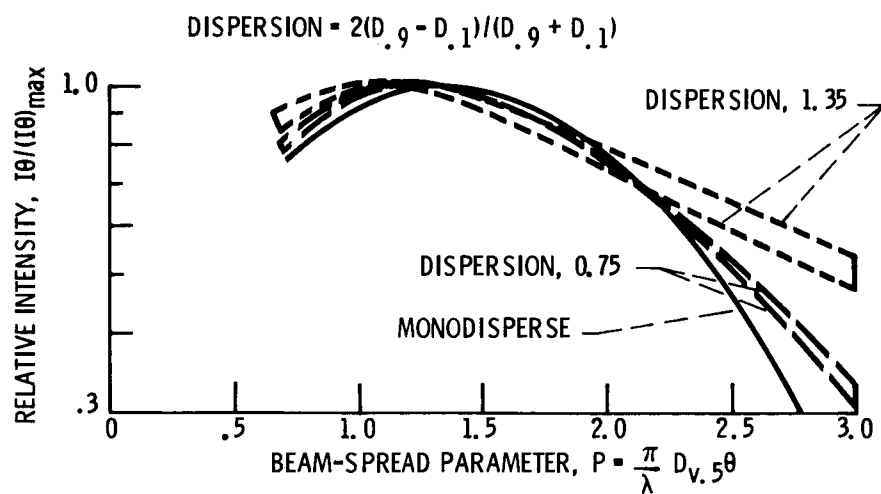
Figure 9. - Envelope of scattered light for five volume-distribution functions and three dispersions.

CD-85-17629
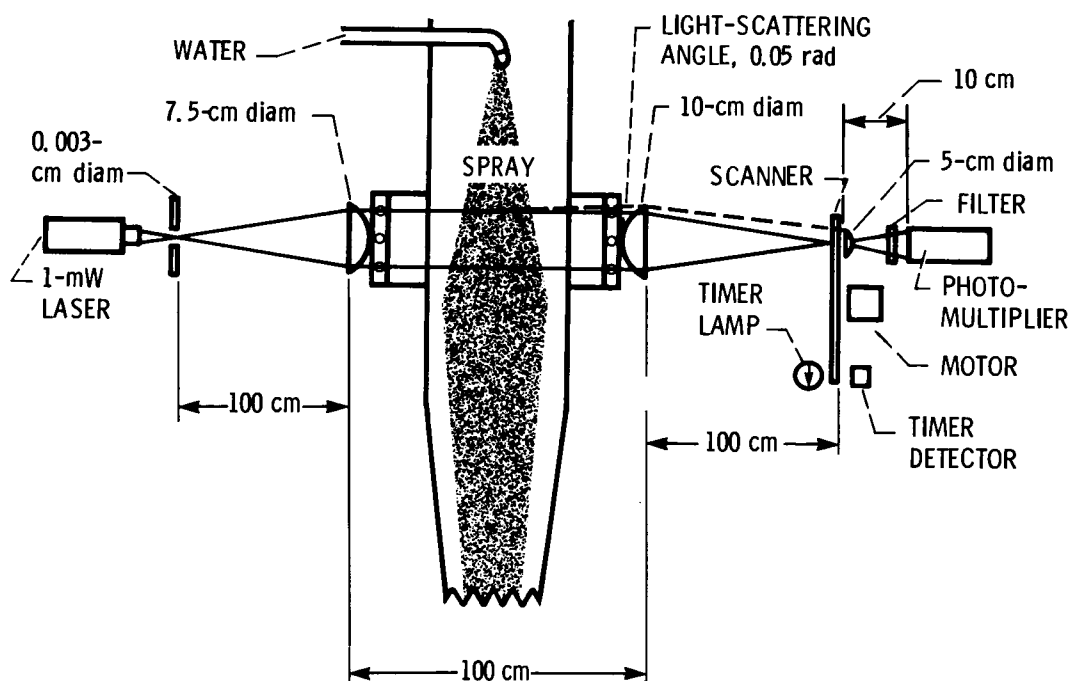
Figure 10. - Lewis Scanning Radiometer spray analyzer.

CD-85-17632

77
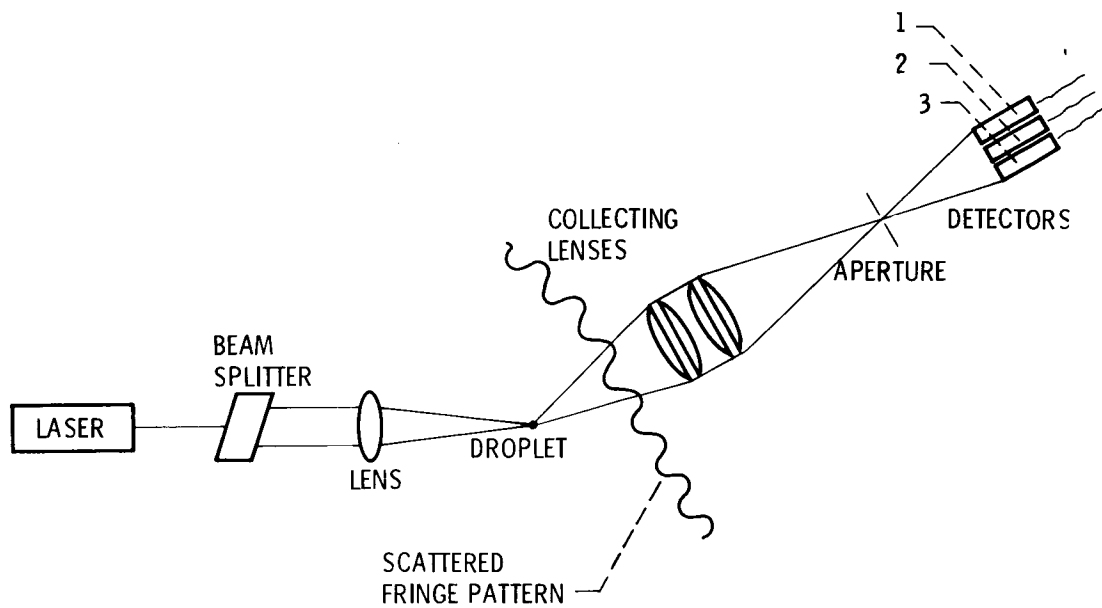
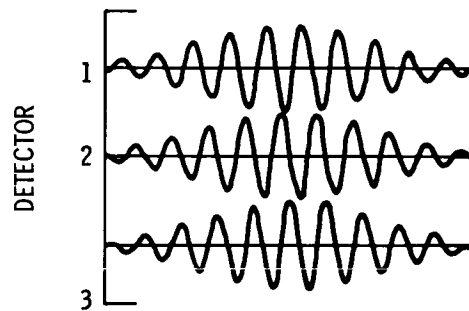Figure 11. - Phase/Doppler detection technique.

CD-85-17395
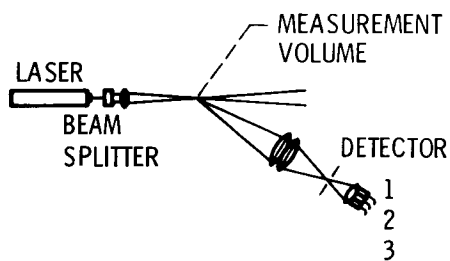
(a) Optical system.
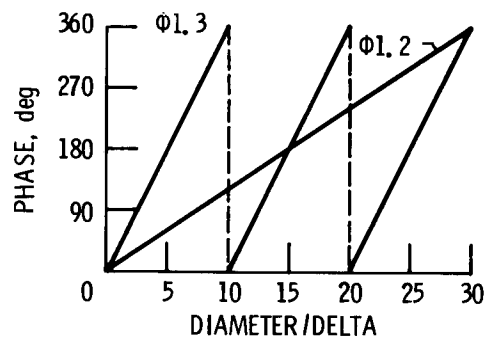
(b) Instrument response curves.

PHASE, deg

360
270
180
90
0

0 5 10 15 20 25 30

DIAMETER/DELTA

Φ1,3

Φ1,2
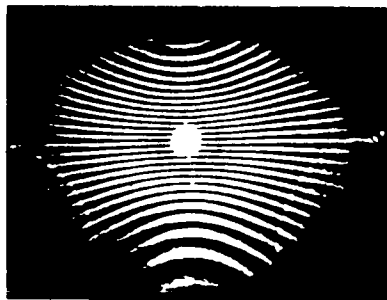
CD-85-17631

(c) Scattered-light interference pattern.

(d) Filtered Doppler burst signals.

Figure 12. - Schematic of Phase/Doppler Spray Analyzer technique.

78
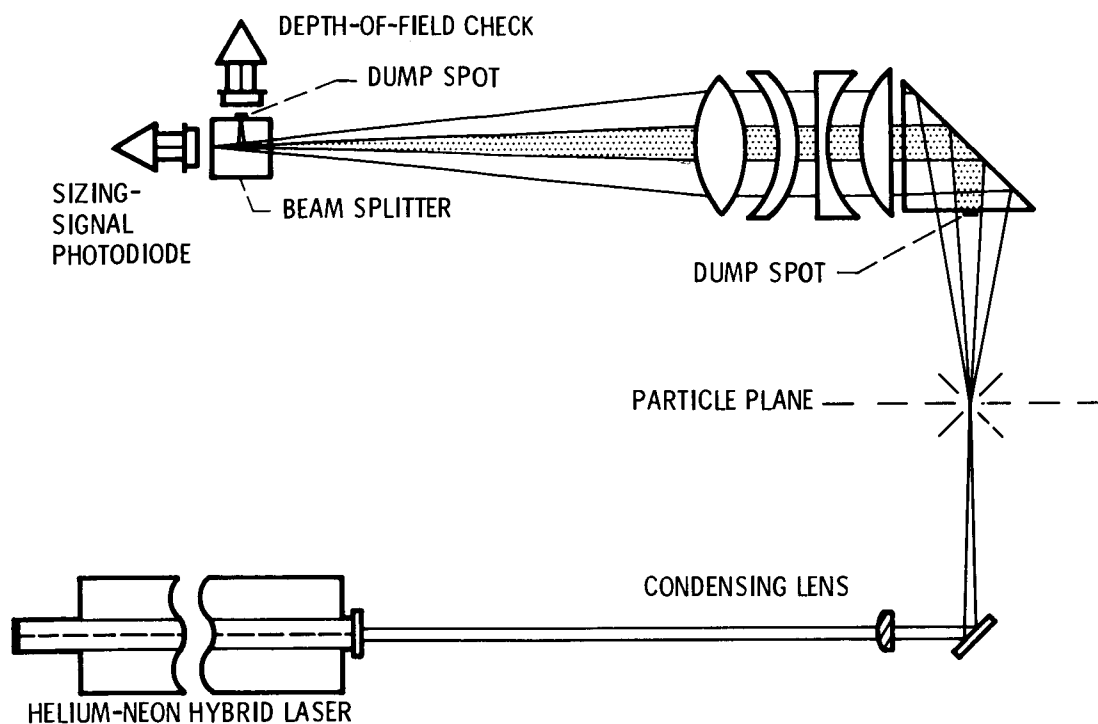
Figure 13. - FSSP optical path.

CD-85-17405
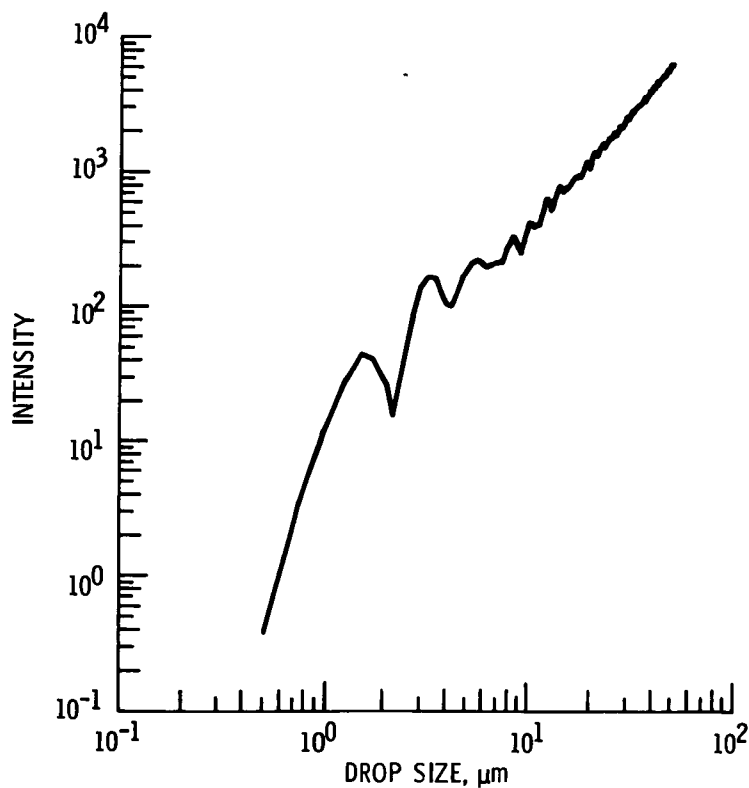
CD-85-17398

Figure 14. - Forward-Scattering Spectrometer Probe (FSSP) light scattering as function of drop size. Light intensity measured at scattering angles of 4° to 14°.

79

COLLIMATED
LIGHT BEAM

SAMPLING
AREA

FLIGHT
DIRECTION

VIEWING
VOLUME

SAMPLED
VOLUME

AREA SEEN
BY ARRAY

INTERMEDIATE SHADOW PLANE
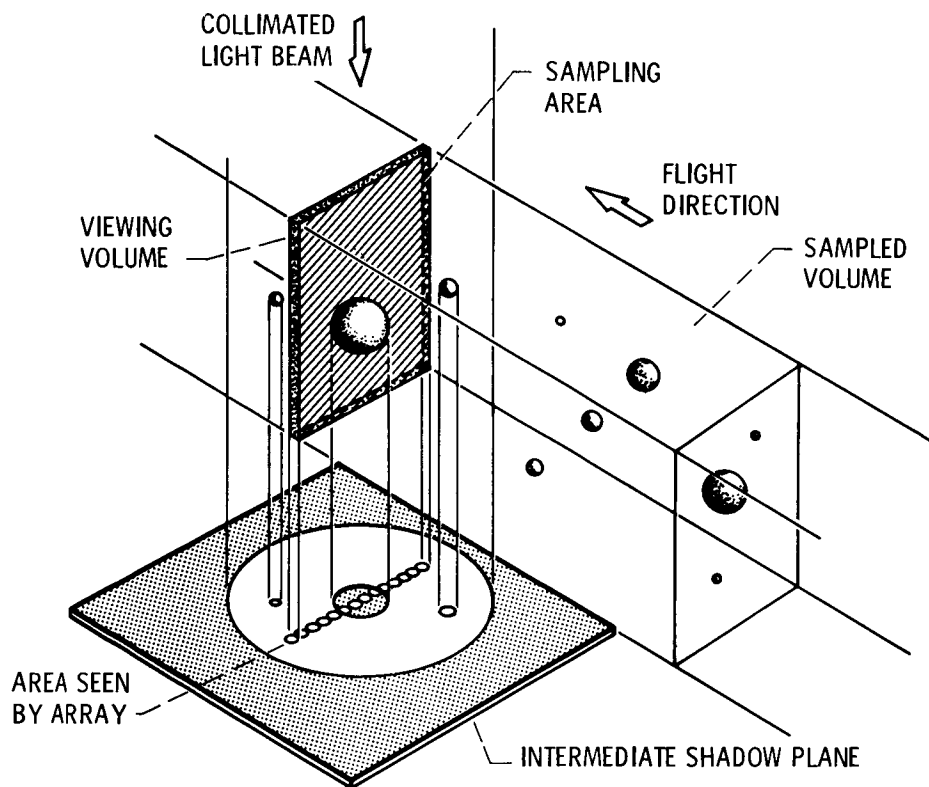
Figure 15. - Optical Array Probe (OAP) operating principle.

MIRROR

>2.0-mW HELIUM-NEON LASER

CONDENSING
LENS; F = 320 mm

PHOTODIDE
ARRAY

SECONDARY
ZOOM LENS

OBJECTIVE
LENS; F = 60 mm

MIRROR
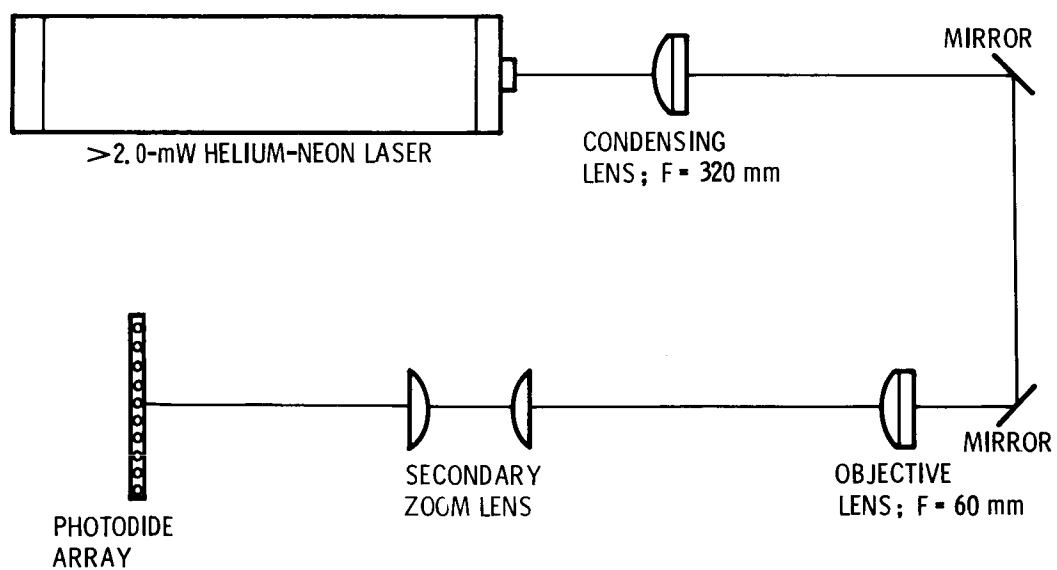
Figure 16. - Optical Array Probe (OAP) optical path.
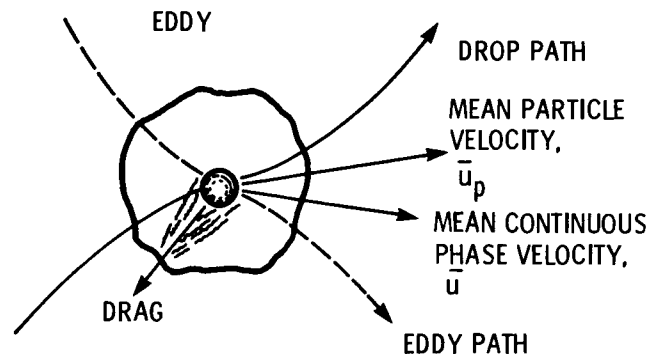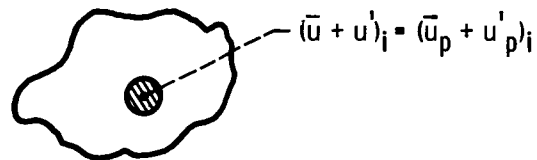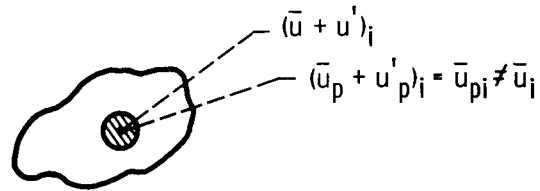
Figure 17. – Phase interactions for particle-laden flow.

$$(\bar{u} + u')_i = (\bar{u}_p + u'_p)_i$$

Figure 18. – Locally homogeneous flow (LHF) model.

ASSUMPTION: FINITE INTERPHASE TRANSPORT
RATES BUT PARTICLES ONLY
RESPOND TO MEAN MOTION

$$\overline{(u + u')}_i$$

$$(\overline{u}_p + u'_p)_i = \overline{u}_{pi} \neq \overline{u}_i$$

NOTES: I - PARTICLE DISPERSION IGNORED - ONLY
VALID FOR "LARGE" PARTICLES

II - MOST WIDELY USED APPROXIMATION
IN CURRENT MODELS OF COMBUSTING
SPRAYS AND PULVERIZED COAL

III - FLOW FIELD FOUND FROM EULERIAN
CALCULATION WITH DISTRIBUTED SOURCE
TERMS DUE TO PARTICLES. LAGRANGIAN
CALCULATION DETERMINES PARTICLE
TRAJECTORIES

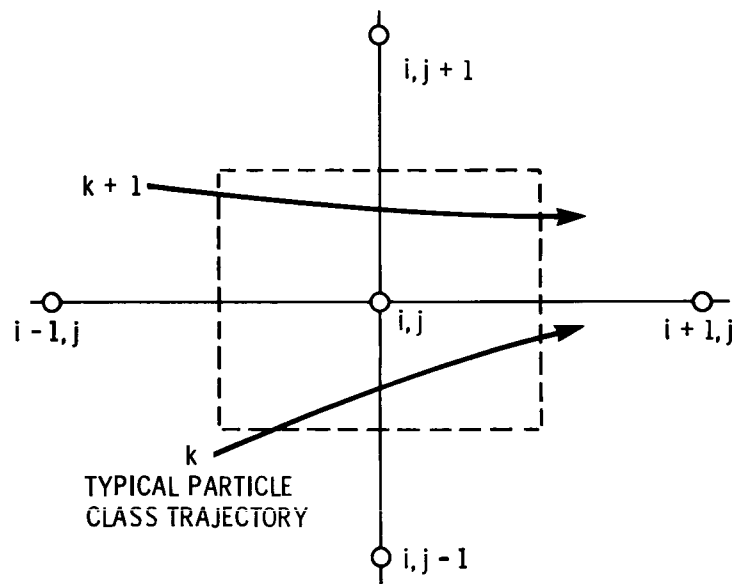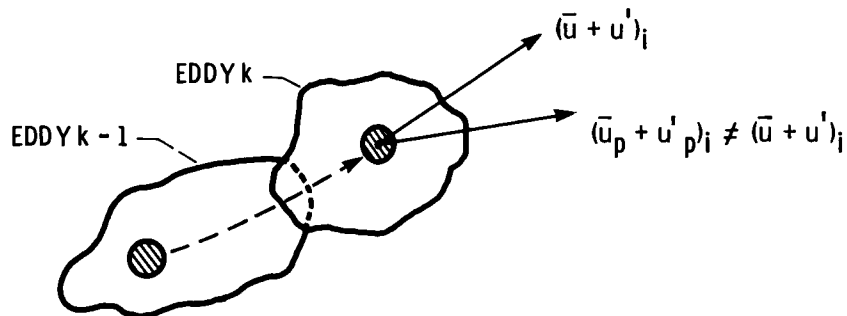Figure 19. - Deterministic separated flow (DSF) model.

CD-85-17406

Figure 20. - Gas-flow computational cell.

CD-85 17408

82

ASSUMPTION: FINITE, INTERPHASE TRANSPORT RATES WITH PARTICLES
INTERACTING WITH INDIVIDUAL EDDIES WHOSE PROPERTIES
ARE FOUND BY RANDOM SAMPLING OF LOCAL TURBULENCE
PROPERTIES

$(\bar{u} + u')_i$

EDDY k

EDDY k - 1

$(\bar{u}_p + u'_p)_i \neq (\bar{u} + u')_i$

NOTES: I - INVOLVES ADDITIONAL ASSUMPTIONS CONCERNING THE
PROPERTIES, SIZE, AND LIFETIME OF EDDIES

II - COMPUTATIONS SIMILAR TO DSF MODELS, BUT MONTE CARLO
TECHNIQUES USED TO FIND STATISTICALLY SIGNIFICANT
NUMBER OF PARTICLE TRAJECTORIES - CAUSING ADDED
COMPUTATIONS

Figure 21. - Stochastic separated flow (SSF) model.
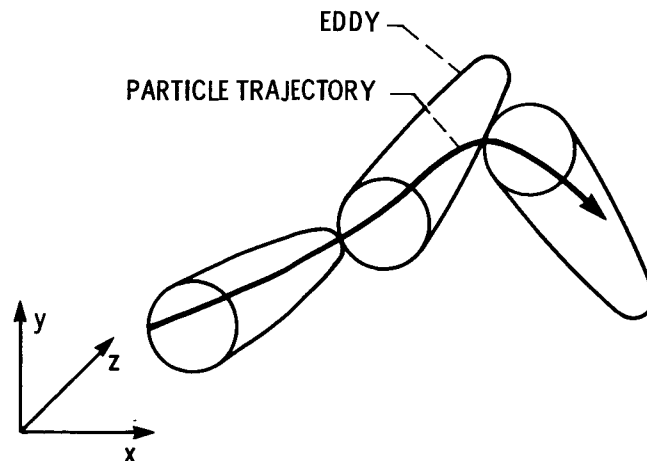
CD-85-17411

EDDY

PARTICLE TRAJECTORY

y

z

x

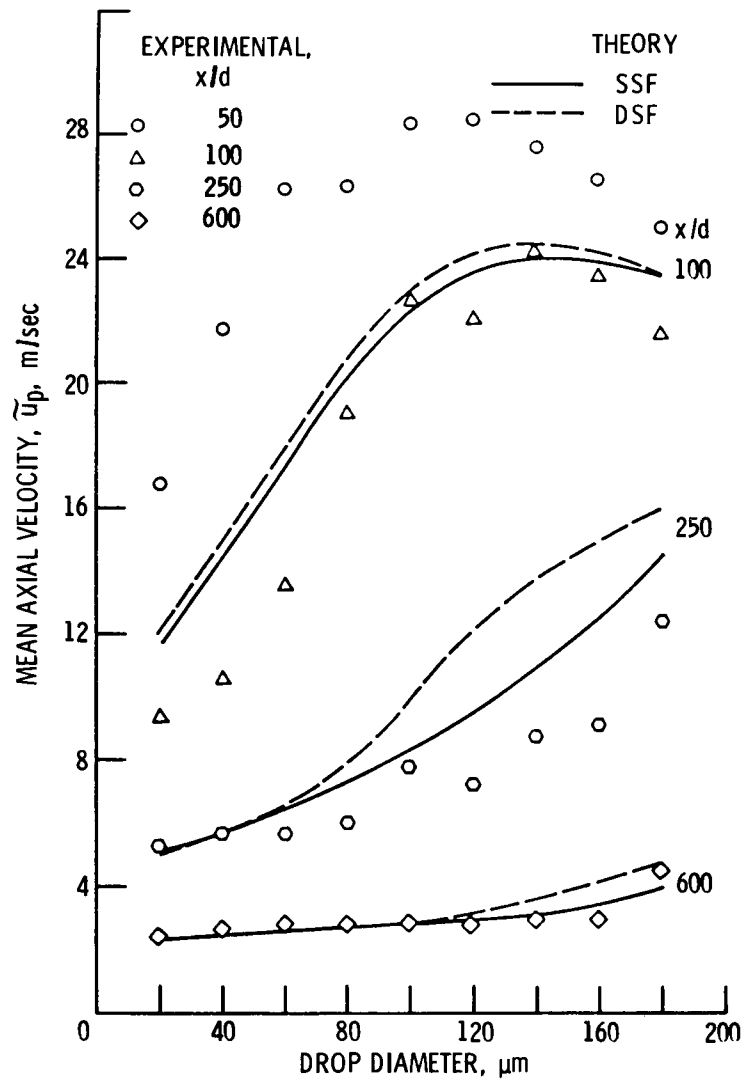Figure 22. - Particle-eddy interaction.

CD-85-17407

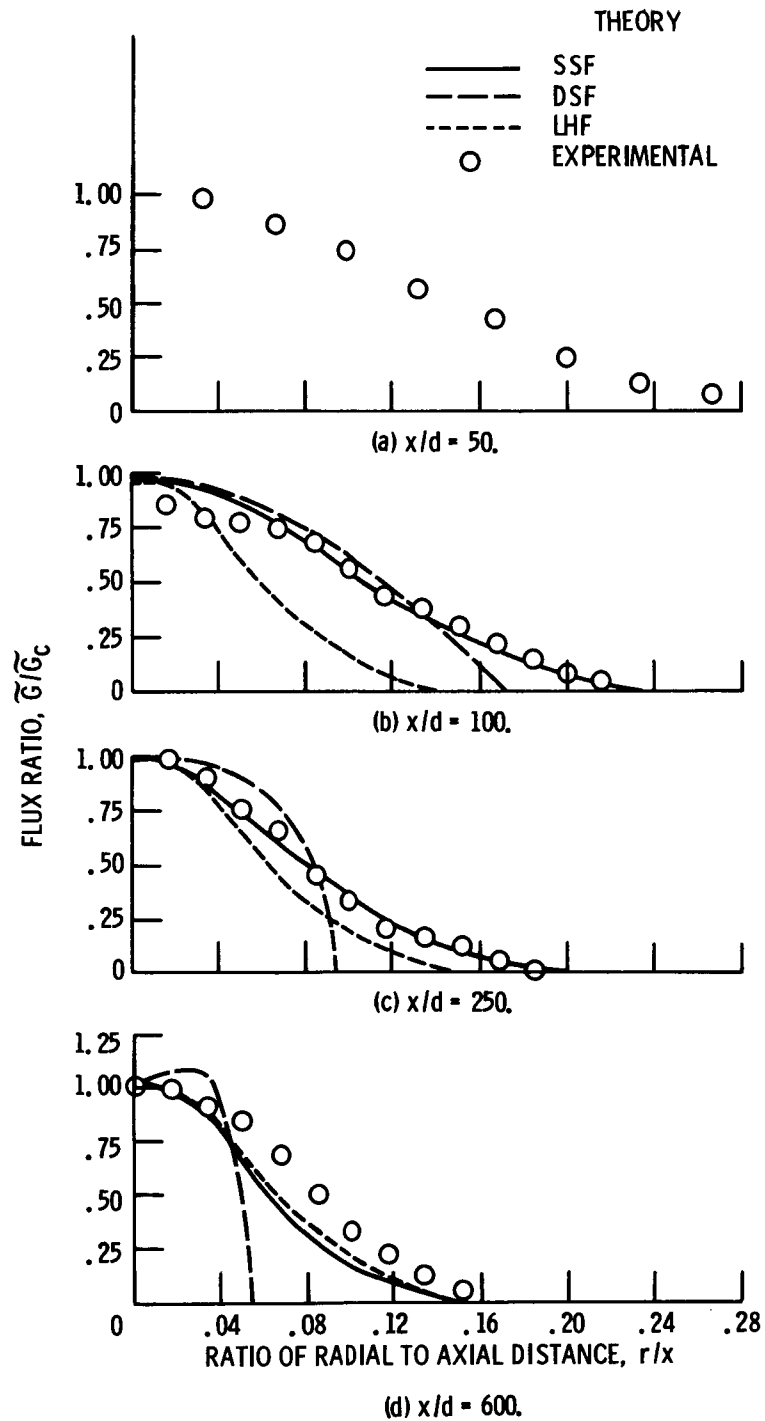Figure 23. - Mean axial-drop velocities along axis. Non-evaporating spray; case 2.

Figure 24. - Radial variation of mean liquid flux. Non-evaporating spray; case 1.
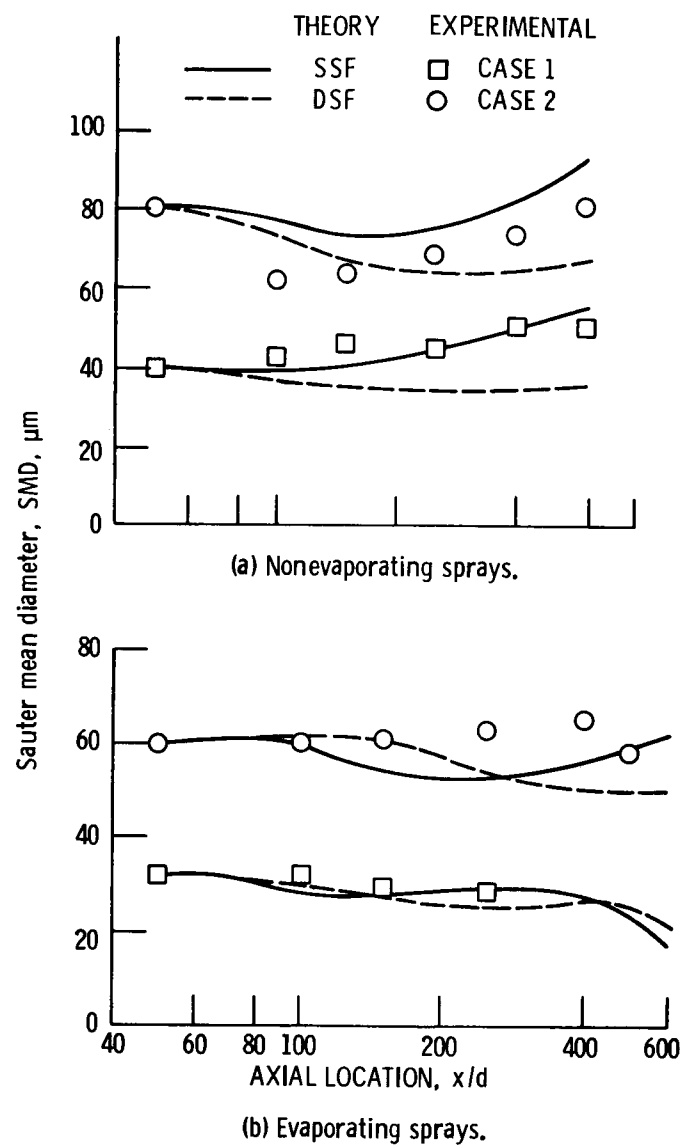
THEORY   EXPERIMENTAL

——— SSF   □ CASE 1

– – – DSF   ○ CASE 2

Sauter mean diameter, SMD, μm

(a) Nonevaporating sprays.

AXIAL LOCATION, x/d

(b) Evaporating sprays.

Figure 25. – Sauter mean diameter (SMD) along axis.

86

MOVABLE SCREENED ENCLOSURE

LDA RECEIVING OPTICS

MINICOMPUTER

TERMINAL

INJECTION TUBE WITH
AXIAL TRAVERSE

LDA SENDING OPTICS

COUNTER

2-W ARGON-ION LASER

EXHAUST

rms
VOLTMETER

ENCLOSURE TRACK
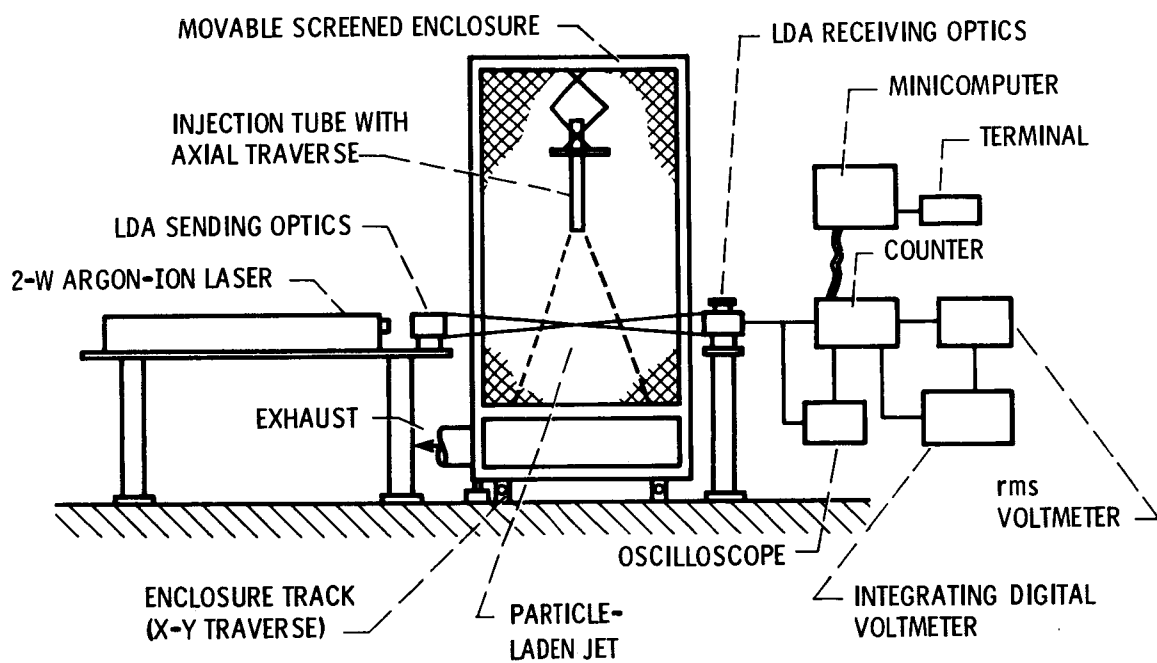(X-Y TRAVERSE)

PARTICLE-
LADEN JET

OSCILLOSCOPE

INTEGRATING DIGITAL
VOLTMETER

Figure 26. - Particle-laden swirling-flow experiment.